A first-principle analysis on the phase stabilities, chemical bonds and band gaps of wurtzite structure $A_x Zn_{1-x}O$ alloys (A = Ca, Cd, Mg)

A first-principle analysis on the phase stabilities, chemical bonds and band gaps of wurtzite structure $A_x Zn_{1-x}O$ alloys (A = Ca, Cd, Mg)

X F Fan[1]**, H D Sun**[1]**, Z X Shen**[1]**, Jer-Lai Kuo**[1] **and Y M Lu**[2]

[1] School of Physical and Mathematical Sciences, Nanyang Technological University, Singapore 637371, Singapore
[2] Key Laboratory of Excited State Processes, Changchun Institute of Optics, Fine Mechanics and Physics, Chinese Academy of Sciences, Changchun 130033, People's Republic of China

E-mail: jlkuo@ntu.edu.sg

Abstract
The phase stabilities and structural and electronic properties of three zinc-based oxide alloy systems ($Ca_x Zn_{1-x}O$, $Cd_x Zn_{1-x}O$ and $Mg_x Zn_{1-x}O$) are studied by first-principle methods. We examine all alloy configurations in three 16-atom supercells ($1 \times 1 \times 2$ B1 phase structure, $2 \times 2 \times 1$ and $2 \times 1 \times 2$ B4 phase structures) and utilize symmetry of the bulk materials to reduce the amount of calculation. Taking into account the contribution of the alloy statistics, we have drawn the regions of phase stability for $Ca_x Zn_{1-x}O$ ($0.25 < x < 0.375$), $Mg_x Zn_{1-x}O$ ($0.375 < x < 0.5$) and $Cd_x Zn_{1-x}O$ ($0.75 < x < 0.875$). We have also analyzed lattice constants (a and c), structural parameter u and the bond lengths in the wurtzite phases. We found that the averaged lattice constants of $Mg_x Zn_{1-x}O$ and $Ca_x Zn_{1-x}O$ do not follow the Vegard rule and this is related to the degree of instability of the wurtzite MgO and CaO. Wurtzite CaO is not stable and turns into hexagonal CaO upon geometry optimization. The calculated band gaps are found to be consistent with the experimental values for alloys $Cd_x Zn_{1-x}O$ and $Mg_x Zn_{1-x}O$. The bowing parameters for alloys $Mg_x Zn_{1-x}O$ and $Cd_x Zn_{1-x}O$ are estimated to be 0.87 and 1.30 eV, respectively.

(Some figures in this article are in colour only in the electronic version)

1. Introduction

Following the group III nitrides (AlN, GaN, InN) and their alloys, ZnO has attracted much attention as a candidate material for light emitting devices (LEDs) and laser diodes (LDs) in the wavelength range from blue–green to ultraviolet due to its unique physical properties, especially the large exciton binding energy (60 meV) [1–4]. An important step toward the development of ZnO-based optoelectronic devices [5] is the fabrication of ZnO-based alloy semiconductors with flexible band-gap engineering that allows for the construction of quantum wells and superlattices [6].

$Be_x Zn_{1-x}O$, $Mg_x Zn_{1-x}O$ and $Ca_x Zn_{1-x}O$ are possible candidates to achieve wider band-gap modification. While a lot of experimental work on $Mg_x Zn_{1-x}O$ [7–22] has been carried out, the fabrication of $Be_x Zn_{1-x}O$ is hindered by the high degree of toxicity of BeO and it was reported only recently by Ryu *et al* [23]. In the theoretical community, $Mg_x Zn_{1-x}O$ alloy [24, 25] has also received more attention than $Be_x Zn_{1-x}O$. Our recent studies found that the solubility of $Mg_x Zn_{1-x}O$ is still better than $Be_x Zn_{1-x}O$ in the Zn-rich region, although ZnO and BeO have the same wurtzite structure [26]. $Ca_x Zn_{1-x}O$ is another candidate to achieve a wider band, but has remained under-explored. To gain ZnO-based optoelectronic materials in the whole visible–ultraviolet emission region from 1.8 to 3.3 eV [6], extensive experimental effects have been made on $Cd_x Zn_{1-x}O$ for narrower band-gap modification [27–37]. A number of first-principle calculations

1

on the properties of the parent compounds CaO [38–40], CdO [41–43], MgO [44, 45] and ZnO [46–48] in the different structures (wurtzite and rock-salt) have appeared in the literature [49–54]. However, as far as we know, the crystal structure and stability of these ternary alloys, $Ca_xZn_{1-x}O$ and $Cd_xZn_{1-x}O$, still have not been well studied except for $Mg_xZn_{1-x}O$ alloy [24, 25].

Unlike III–N nitrides, which all assume the same wurtzite structures, thermodynamically stable II–O oxides can be either wurtzite structures (ZnO, BeO) or rock-salt structures (CaO, CdO, MgO) [55, 56]. The ternary Zn-based oxide alloys ($Ca_xZn_{1-x}O$, $Cd_xZn_{1-x}O$ and $Mg_xZn_{1-x}O$) are made from the nonisostructural components (rock-salt +wurtzite). Therefore, in Zn-based ternary oxide alloys, the structure phase separation will occur in some transition concentration. For example, both experimental [57] and theoretical [24, 25] investigations have shown that the stability of alloy $Mg_xZn_{1-x}O$ with wurtzite structure is up to $x \leqslant 1/3$. For wurtzite $Cd_xZn_{1-x}O$ alloy, different stability ranges were obtained with varying growth methods. So far, the maximal Cd concentration with stable wurtzite structural $Cd_xZn_{1-x}O$ phase has been achieved by Ishihara *et al* with $x \leqslant 0.69$ [36]. For $Ca_xZn_{1-x}O$ alloy, to our knowledge, there has been no experimental and theoretical analysis for the phase stability. One of our main motivations in this work is to engage the systematical first-principle calculations to compare the stability of B4 phase (wurtzite structure) in the above-mentioned II–VI oxide alloys. The results are expected to shed some light on the fundamental understanding of physical properties in these nonisostructural alloy systems and serve as references for future experimental analysis. Moreover, we have investigated chemical, structural and electronic properties in these alloys. These structural and electronic properties are crucial for the heterostructure design and optimized growth of the related quantum wells and superlattices.

This paper is organized as follows. In section 2 the detailed calculation methods and the theoretical model for the construction and analysis of alloy structures used in our work are described. The main results of this work are presented in section 3. Finally, a brief summary is given in section 4.

2. Computational methods and theoretical model

The effects of disorder on the stability and structure of alloys has gained considerable attention over the past few decades. Simple single-site theory, such as the coherent-potential approximation (CPA) [58], based on the average occupation of the substitution atoms, often brings about some deviation from the actual physical properties. The importance of the local chemical environment such as charge transfer and local structural relaxation in different configurations for determining the thermodynamics and electronic properties of an alloy has been noted. Zunger *et al* [59, 60] has shown that the most important physical properties can be analyzed correctly just by considering the correlation of nearby neighbors. In order to include the local correlations, in the present work, the calculation and analysis are carried out in several supercells with 16 atoms. For the B1 phase (rock-salt structure) unit cell,
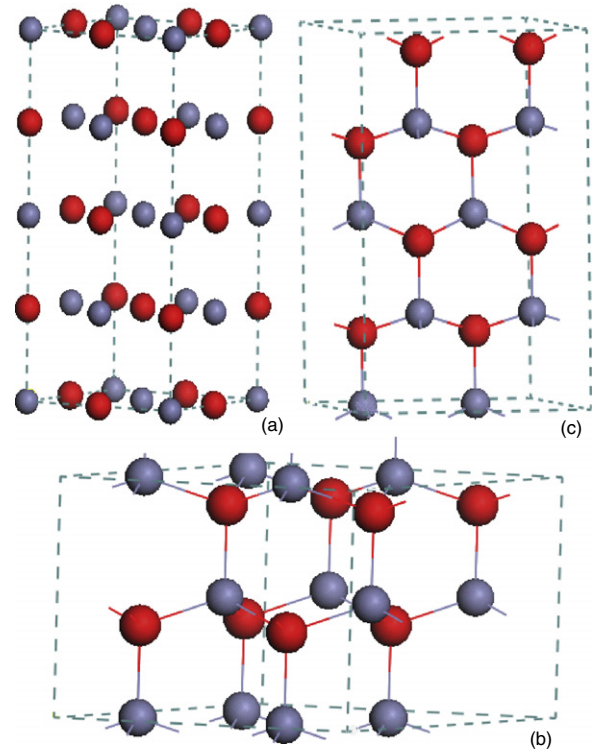
Figure 1. Illustration of $1 \times 1 \times 2$ B1 phase supercell (a), $2 \times 2 \times 1$ B4 phase supercell (b) and $2 \times 1 \times 2$ B4 phase supercell (c). Red spheres represent the O atoms and gray spheres represent the Zn atoms.

with space group $Fm\bar{3}m$, a $1 \times 1 \times 2$ supercell (shown in figure 1(a)) is used. For the B4 phase unit cell, with space group $P6_3mc$, we have considered two supercells along [001] and [100] directions as shown in figures 1(b) and (c). The $2^8 = 256$ configurations in each of the three supercells have been simplified by eliminating the symmetrically equivalent ones. For the $1 \times 1 \times 2$ supercell of the B1 phase, there are 27 symmetrically distinct configurations. For the B4 phase, we found 22 and 34 symmetrically distinct configurations in the $2 \times 2 \times 1$ and $2 \times 1 \times 2$ supercells, respectively. The degeneracy factors of all the above-mentioned configurations are detailed in table 1.

The Helmholtz free energy in determining the stability of the system can be divided into two parts, namely the mixing energy (the formation enthalpy) ΔE and the mixing entropy ΔS, by the formula [61]

$$\Delta F(x, T) = \Delta E(x, T) - T \Delta S(x, T). \quad (1)$$

At zero temperature, the relative stability of an alloy configuration can be estimated by the calculation of the formation enthalpy, which is defined as the difference in energy between the alloy and the weighted sum of the constituents. For the parents with the same phase (α), such as group-III nitride alloys, the formation enthalpy of the alloy configuration (σ) can be shown by the formula

$$\Delta E_\alpha(\sigma, x) = E_\alpha(\sigma, A_xB_{1-x}C) - xE_\alpha(AC) - (1-x)E_\alpha(BC), \quad (2)$$

Table 1. All symmetrically distinct alloy configurations in $1 \times 1 \times 2$ rock-salt, $2 \times 2 \times 1$ wurtzite and $2 \times 1 \times 2$ wurtzite supercells (defined in figure 1). #(A) indicates the number of A atoms in the alloy configuration and g_j is the degeneracy factor defined in equation (4).

$1 \times 1 \times 2$ rock-salt			$2 \times 2 \times 1$ wurtzite			$2 \times 1 \times 2$ wurtzite		
No	#(A)	g_j	No	#(A)	g_j	No	#(A)	g_j
0	0	1	0	0	1	0	0	1
1	1	8	1	1	8	1	1	8
2	2	4	2	2	12	2	2	4
3	2	4	3	2	12	3	2	4
4	2	16	4	2	4	4	2	8
5	2	4	5	3	8	5	2	4
6	3	8	6	3	24	6	2	8
7	3	16	7	3	24	7	3	8
8	3	16	8	4	2	8	3	16
9	3	16	9	4	6	9	3	8
10	4	32	10	4	8	10	3	16
11	4	4	11	4	24	11	3	8
12	4	8	12	4	6	12	4	16
13	4	8	13	4	24	13	4	16
14	4	6	14	5	24	14	4	2
15	4	8	15	5	8	15	4	4
16	4	4	16	5	24	16	4	8
17	5	16	17	6	12	17	4	2
18	5	16	18	6	12	18	4	4
19	5	8	19	6	4	19	4	8
20	5	16	20	7	8	20	4	2
21	6	4	21	8	1	21	4	8
22	6	4				22	5	8
23	6	4				23	5	16
24	6	16				24	5	8
25	7	8				25	5	8
26	8	1				26	5	16
						27	6	4
						28	6	4
						29	6	8
						30	6	4
						31	6	8
						32	7	8
						33	8	1

where $x(\sigma)$ is the concentration of configuration σ. For nonisostructural compounds, with $E_\alpha(\text{AC}) < E_\beta(\text{AC})$ and $E_\beta(\text{BC}) < E_\alpha(\text{BC})$, the formation enthalpy is expressed as [25]

$$\Delta E_{\alpha,\beta}(\sigma, x) = E_\gamma(\sigma, A_x B_{1-x} C)$$
$$- x E_\alpha(\text{AC}) - (1 - x) E_\beta(\text{BC}), \qquad (3)$$

where γ can be either α or β phase.

The averaged structural and electronic properties as a function of concentration can be analyzed by considering the contribution of all the alloy configurations with the same concentration and using the following formula:

$$\langle P(x) \rangle = \sum_{i=1, i\,\text{max}} g_i P_i \Big/ \sum_{i=1, i\,\text{max}} g_i, \qquad (4)$$

where P_i is the property of the ith configuration and g_i is the degeneracy factor. Note that the summation in equations (4) is limited to those configurations with concentration x.

In the present work, the structural and electronic properties of all the alloy configurations described above

are examined by the density functional theory (DFT) and the local density approximation (LDA) [62, 63] along with the projector augmented wave (PAW) method [64, 65] as implemented in the VASP program package [66–68]. The PAW potentials used for cadmium and zinc treat 4p electrons in the valence. The k-space integral and plane-wave basis, as detailed below, are tested to ensure the total energy is converged at the 1 meV/cation level. An energy cut-off of $E_{\text{cut}} = 1200$ eV is sufficient for the different supercells of the three alloys ($Ca_x Zn_{1-x}O$, $Cd_x Zn_{1-x}O$ and $Mg_x Zn_{1-x}O$), while the different k points are chosen for the different supercells. For the $1 \times 1 \times 2$ supercell of the B1 phase, a $4 \times 4 \times 2$ Monkhorst–Pack type mesh [69] is chosen in the first Brillouin zone. With regard to the B4 phase, the $3 \times 3 \times 4$ and $3 \times 5 \times 3$ Monkhorst–Pack type mesh [69] is chosen for the $2 \times 2 \times 1$ and $2 \times 1 \times 2$ supercells, respectively. In order to enable the alloy configurations to converge to their most stable conformation, all atomic positions and the lattice constants are relaxed. The total energies are obtained after the geometrical optimization is finished. The Γ-point band gap is estimated after a self-consistent calculation that can generate high quality charge density is finished with the optimized geometrical structure.

3. Results and discussion

3.1. Structures of the parent compounds

Before handling the main steps of the present work, let us analyze the basic properties of the pure bulk materials (CaO, CdO, MgO and ZnO). The wurtzite structure, which contains two formula units per primitive cell, requires three parameters to specify with space group $P6_3mc$. These parameters are the lattice constant a, c (or the c/a ratio) and the dimensionless internal structural parameter u, which is defined as the ratio of the length of the bond parallel to the c axis to the lattice constant c. In ideal wurtzite structure characterized by equal bond lengths, c/a and u are 1.6333 and 3/8, respectively. For the rock-salt structure, the only degree of freedom required is the lattice constant a, since anion and cation occupy two different fcc lattice sites, respectively.

The calculated equilibrium structural parameters of wurtzite and rock-salt CaO, CdO, MgO and ZnO are listed in table 2 along with some experimental values for comparison. For the rock-salt structures, all the calculated values agree with the experimental ones within 2%. Hence, it is expected that the lattice parameters of the alloys can be described with similar accuracy in our calculation method. For wurtzite structures, we found that the agreement between our calculation and extensive experimental measurements on ZnO is of the same accuracy as those in the rock-salt form.

While the wurtzite CaO, CdO and MgO have not been successfully synthesized yet, our calculations reveals an interesting trend, that the stability of a wurtzite phase (that is ZnO > CdO > MgO > CaO) is correlated with its deviation from the ideal wurtzite values. Our calculations show that wurtzite CdO is stable, with u (0.385) and c/a ratio (1.582) sufficiently close to the ideal values. The instability of wurtzite MgO and the possibility of spontaneous relaxation to the h-MgO structure (a hexagonal form of MgO where the puckered

Table 2. The LDA-optimized lattice constants a and $c(c/a)$, internal dimensionless parameter u and volume percent anion–cation pair V of CaO, CdO, MgO and ZnO with wurtzite and rock-salt structures. The (c/a) and u values for a perfect wurtzite structure are 1.6333 and 0.375 respectively. Some experimental data in the literature are listed for comparison.

Compound	a (Å)		c (Å) (c/a)		u		V (Å³/pair)
	LDA	Exp.	LDA	Exp.	LDA	Exp.	LDA
CaO ('wurtzite')	3.8939		4.6755 (1.201)		0.4997		30.70
CaO (rock-salt)	4.6942	4.81[a]					25.86
CdO (wurtzite)	3.5817		5.6659 (1.582)		0.3849		31.47
CdO (rock-salt)	4.6561	4.696[b]					25.23
MgO (wurtzite)	3.2786		4.8736 (1.486)		0.4046		22.68
MgO (rock-salt)	4.152	4.212[c]					17.89
ZnO (wurtzite)	3.2032	3.283[d]	5.1386 (1.604)	5.309[d]	0.3814	0.3786[d]	22.83
		3.258[e]		5.220[e]		0.382[e]	
ZnO (rock-salt)	4.2110	4.275[f], 4.278[g], 4.271[h], 4.283[i]					18.67

[a] Reference [77]. [b] Reference [79]. [c] Reference [81]. [d] Reference [78]. [e] Reference [80]. [f] Reference [82]. [g] Reference [78].
[h] Reference [80]. [i] Reference [83].

wurtzite (001) layers are leveled out, leading to $u = 0.5$) were discussed in the literatures [70, 71]. In our $2 \times 2 \times 1$ and $2 \times 1 \times 2$ unit cell, wurtzite MgO remains as a stable minimum with a small barrier that separates the wurtzite MgO and the h-MgO structure. Such instability of wurtzite MgO is consistent with the significant deviation of u (0.405) and c/a ratio (1.486) from the ideal values. In our calculation wurtzite CaO is not stable in both $2 \times 2 \times 1$ and $2 \times 1 \times 2$ unit cells, where the wurtzite CaO relaxes to h-CaO structure with $u = 0.5$ spontaneously. We will come back to this issue in section 3.2, where we shall analyze the stability of $Mg_xZn_{1-x}O$ and $Ca_xZn_{1-x}O$.

3.2. Formation enthalpy and phase stability

It is found that fourfold-coordinated (CN4) B4 phase (wurtzite structure) configurations have lower energy than their sixfold-coordinated (CN6) analogs (rock-salt structure) in Zn-rich region and the reverse situation occurs in the Mg- (or Ca-, Cd-) rich region. Since structural phase separation may occur in these alloy systems with different parent crystal structures, the analysis of the phase transition point is an important issue. The crossover of the CN4–CN4 and CN6–CN6 lines is determined by the end-point energies near $x = 0.43$, 0.46 and 0.59 for alloys $Mg_xZn_{1-x}O$, $Ca_xZn_{1-x}O$ and $Cd_xZn_{1-x}O$, respectively. These crossover concentrations can be regarded as a rough estimate to define the maximum concentration at which wurtzite phases are stable (it would be exact if there is no deviation from the Vegard's rule [72]). The crossover concentration points of alloys $Mg_xZn_{1-x}O$ and $Ca_xZn_{1-x}O$ are smaller (0.43 and 0.46) than that of alloy $Cd_xZn_{1-x}O$ (0.59), which is consistent with the fact that wurtzite MgO and CaO have larger values for the internal parameter u, reflecting the stability of wurtzite structure. Here we should note that the crossover concentration point of alloy $Mg_xZn_{1-x}O$ (0.43) is smaller than that of $Ca_xZn_{1-x}O$, which is due to the use of h-CaO structure in the calculation (note that wurtzite CaO is not stable and tends to relax to h-CaO).

Beyond the Vegard's rule, we have calculated the total energy of all alloy configurations in the $1 \times 1 \times 2$ supercell of the B1 phase and the $2 \times 2 \times 1$ and $2 \times 1 \times 2$ supercells of the B4 phase, respectively. Formation enthalpies of

these alloy configurations for $Ca_xZn_{1-x}O$, $Cd_xZn_{1-x}O$ and $Mg_xZn_{1-x}O$ are depicted in figure 2. For $Ca_xZn_{1-x}O$ and $Cd_xZn_{1-x}O$, significant deviation from Vegard's rule with $\Delta E_{B1} > 0$ and $\Delta E_{B4} > 0$ is apparent. The positive formation (mixing) enthalpy can be well understood by large size mismatch between the atomic constituents (Zn^{2+}, 0.74 Å; Ca^{2+}, 0.99 Å; Cd^{2+}, 0.97 Å). $Mg_xZn_{1-x}O$, on the other hand, has small and negative ΔE_{B1} and ΔE_{B4}, which is consistent with the theoretical calculations reported by Sanati *et al* [25] and the commonly accepted notion that there is less volume deformation in $Mg_xZn_{1-x}O$ as a result of the compatible sizes of Mg (Mg^{2+}: 0.72 Å) and Zn (Zn^{2+}: 0.74 Å) ions.

Taking into account these alloy configurations, we can draw a region of phase transition for three alloys (depicted by the arrows in figure 2). For alloy $Mg_xZn_{1-x}O$, the region is approximately $0.375 < x < 0.5$ as shown in figure 2(c). The lower limit ($x = 0.375$) is consistent with the result of experiment and other theoretical calculations for the stable wurtzite structure [24, 25, 57]. The calculated phase transition region is consistent with the recent experimental mixing region of two phases ($0.34 < x < 0.65$) by Vashaei and coworkers [19]. For $Cd_xZn_{1-x}O$ and $Ca_xZn_{1-x}O$, the regions are approximately $0.75 < x < 0.875$ and $0.25 < x < 0.375$, as shown in figures 2(b) and (a). The stable wurtzite $Cd_xZn_{1-x}O$ with $x \leqslant 0.69$ reported recently by Ishihara *et al* [36] is consistent with the wurtzite stable region of the theoretical calculation here. The large stable region of wurtzite $Cd_xZn_{1-x}O$ seems understandable because pure crystal CdO has relatively stable wurtzite structure, as shown in table 2.

The enthalpies $\Delta E_{B1,B4}$ taken from the most stable form of parent materials are positive for all three alloy systems. This implies that the alloy systems are unstable at zero temperature. As the actual process of material synthesis is carried out at some temperature of several hundred kelvin, the mixing entropy should be considered for analyzing the stability of the alloy system. In a nonmagnetic alloy system, the mixing entropy usually includes the contribution from configuration, vibration modes and electron excitation. Normally, electron excitation has very high characterization temperature, so the mixing entropy induced by electron excitation is small and
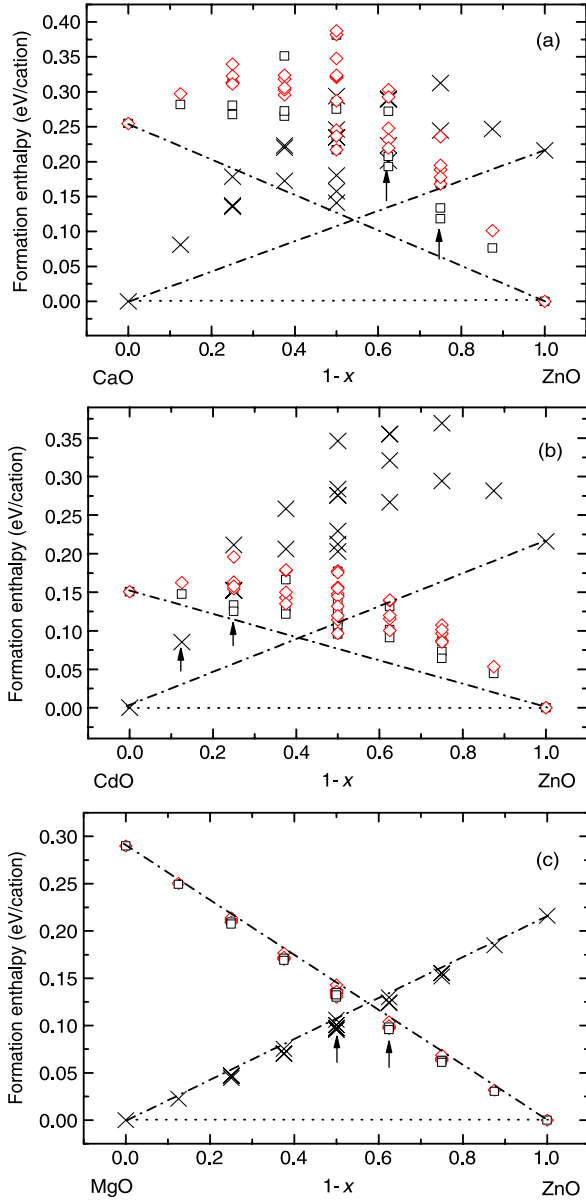
Figure 2. Formation enthalpy of all symmetrically distinct alloy configurations in $1 \times 1 \times 2$ B1 phase supercell (black '×'), $2 \times 2 \times 1$ B4 phase supercell (black square) and $2 \times 1 \times 2$ B4 phase supercell (red empty diamond). Three lines connect the end points for each alloy system: two dash–dot lines for AO (A = Ca, Cd and Mg)–ZnO with B1 phase and B4 phase, one dotted line for AO (B1)–ZnO (B4).

can be ignored. The major part in the mixing entropy comes from the configurations. Considering that the formation enthalpy is in the range of $\sim$100 meV/cation at zero temperature, a temperature as high as $\sim$2000 K is required to counteract the positive formation enthalpy by the mixing entropy induced by the configurations for the three alloy systems. Usually, the mixing entropy by the vibration will reduce the temperature of the thermo-equilibrium state by $\sim$10%. Thus the high temperature needed by the thermo-equilibrium state implies that the alloy system made from the nonisostructural components should be easy to experience phase separation and there will be low solubility for each

parent phase. For the alloy $Mg_xZn_{1-x}O$, this has been confirmed by the observation of the low solubility limit of Mg in ZnO for $Mg_xZn_{1-x}O$ [73]. Actually, the success in fabricating the single-phase alloy with higher concentrations is based on today's epitaxial growth techniques (P-MBE, L-MBE, RP-MOCVD and so on) that allow for the extremely non-equilibrium growth condition. For instance, in the process of the epitaxial growth of the oxide materials by P-MBE, the temperature of the substrate usually is in the range of $\sim$400 to $\sim$1000 K. Under such a low growth temperature, the substrate surface will have an important effect on the lattice relaxation necessary for phase separation. Just as Andrei *et al* [74] considered, the phase separation is kinetically limited [74]. At low temperature, the time the alloy needs to segregate into the parent lower-energy constitutions by lattice relaxation will be much longer than that of the epitaxial growth with a single phase due to the surface transfer of atoms or atomic clusters. So the local single alloy phase would be formed as observed by experiments.

3.3. Structural properties of the alloys in B4 phase

To obtain the statistic average of local environment effect, the structural properties will be analyzed in the $2 \times 2 \times 1$ and $2 \times 1 \times 2$ supercells for wurtzite structure. The lattice constants of all alloy configurations and the averaged lattice constants calculated via equation (4) for $Ca_xZn_{1-x}O$, $Cd_xZn_{1-x}O$ and $Mg_xZn_{1-x}O$ are shown in the upper panels of figure 3(a)–(c), respectively. The agreements between theoretical calculation and the experimental results for alloys $Cd_xZn_{1-x}O$ and $Mg_xZn_{1-x}O$ are comparable with the results of the pure materials (in table 2). The slight underestimate of the lattice constants by theoretical methods is in line with the well known tendency for DFT/LDA to overbind. Furthermore, it should be noted that the lattice constants of different alloy configurations of $Cd_xZn_{1-x}O$ can differ by 0.4 Å at $x = 50\%$. Therefore, appropriate alloy statistics is necessary to faithfully reflect the structural properties.

The averaged lattice constants of the three alloys are compared with linear behavior governed by Vegard's law [72]. For $Cd_xZn_{1-x}O$, we can see that the averaged lattice constants a and c exhibit linear dependence on the concentration. But for alloy $Ca_xZn_{1-x}O$ and $Mg_xZn_{1-x}O$, significant deviation from Vegard's law is obvious. In $Mg_xZn_{1-x}O$, the sudden increase in a (and decrease in c) at $x \sim 0.80$ implies that the wurtzite $Mg_xZn_{1-x}O$ becomes unstable and has a tendency to relax into h-$Mg_xZn_{1-x}O$ (see the discussion on the lattice parameter u later). Similarly, in alloy $Ca_xZn_{1-x}O$, the dramatic change of lattice constant c appearing at $0.375 < x < 0.625$ also means that a structural phase transition (from wurtzite to hexagonal) must occur in this region.

The averaged u for all alloy configurations are shown for the three alloys in the lower panel of figure 3. The concentration dependence of the mean value u exhibits the same trend as that of the lattice constants. This trend is actually the reflection of phase stability as a function of the concentration of A (Ca, Mg, Cd) for wurtzite structure. For example, the mean value u of $Ca_xZn_{1-x}O$ almost reaches 0.5
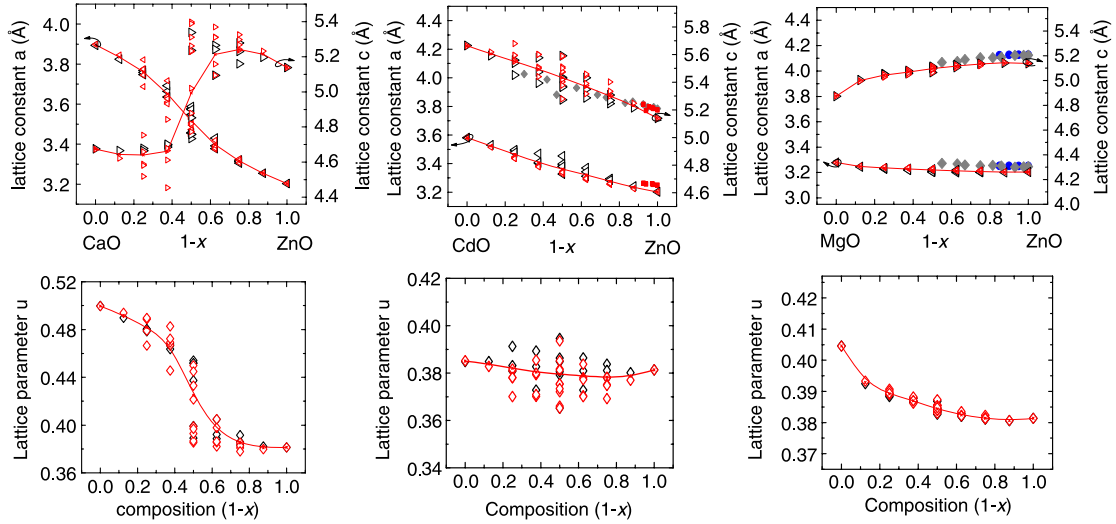
Figure 3. Calculated lattice constants *a* (presented by ◁) and *c* (presented by ▷) of all alloy configurations and averaged lattice constants (red line) for three alloy systems $A_xZn_{1-x}O$ (A = Ca, Cd and Mg) are shown in the upper panels. Experimental data (different symbols) from [22, 57, 5, 36] ($Mg_xZn_{1-x}O$ [22, 57] and $Cd_xZn_{1-x}O$ [5, 36]) are shown for comparison. Lattice parameter *u* of alloy configurations (black diamonds are for $2 \times 2 \times 1$, the red one for $2 \times 1 \times 2$) and averaged lattice parameter (red line) are shown in the lower panels.

for $x > 0.5$. This result combined with the dramatic change of lattice constant *c* is a direct indicator that wurtzite CaO is not stable and the metastable form of pure crystal CaO should be a hexagonal phase. For each configuration of each concentration, the values of lattice parameter *u* have larger variations in alloys $Ca_xZn_{1-x}O$ and $Cd_xZn_{1-x}O$ than $Mg_xZn_{1-x}O$. This phenomenon is partly attributed to the larger ionic radius of Cd^{2+} and Ca^{2+} than that of Zn^{2+} and the close radius of Mg^{2+} to that of Zn^{2+}.

The calculated nearest-neighbor (NN) bond lengths d_{A-O} and d_{Zn-O} for all alloy configurations and the mean values (via equation (4)) are shown in figure 4. The individual NN bond lengths d_{A-O} and d_{Zn-O} in the alloy are found to be closer to the pure bulk values than the concentration weighted average values for the three alloy systems.

It is interesting to note that while the NN Mg–O bond in pure MgO is larger than the NN Zn–O bond in pure ZnO, all the NN Mg–O bonds in alloys are shorter than NN Zn–O bonds in $Mg_xZn_{1-x}O$. While the exact origin is not known, this unique feature implies that the Mg–O bonds are strengthened in the alloy configurations.

3.4. Band gap and bowing parameter

As a fundamental property of the optoelectronic materials, the fundamental energy gaps of the alloys are studied in this part. Since wurtzite CaO, MgO, CdO and ZnO all have the fundamental energy gaps with the $\Gamma_c(min) \rightarrow \Gamma_v(max)$ energy transition, it is reasonable to expect that the three alloy systems with wurtzite structures would have direct band gaps. So the LDA-calculated band gaps of each configuration in the $2 \times 2 \times 1$ and $2 \times 1 \times 2$ supercells are extracted by just analyzing the Γ-point energy levels.

The calculated Γ-point band gaps of the pure compounds CaO, MgO, CdO and ZnO are compared with the experimental values in table 3. The large error in the band gap is a well

Table 3. Band gaps of CaO, CdO, MgO and ZnO with wurtzite and rock-salt structures. The first column shows the band gaps at the Γ point calculated by the LDA method (the calculated value of wurtzite CdO is from [52]). Experimental data in literature are listed in the second column for comparison. The 'predicted' band gaps (shown in the third column) for the thermodynamically unstable forms are obtained by shifting the LDA-calculated band gaps at Γ point by the difference between the LDA-calculated and experimental values of the same oxides in their thermodynamically stable phase.

Compound	LDA	Experiment	'Predicted'
CaO (wurtzite)	3.25		7.63*
Rock-salt	3.42	7.8[c]	
CdO (wurtzite)	−0.34[a]		0.91*
Rock-salt	1.03	2.28[b]	
MgO (wurtzite)	3.53		6.34*
Rock-salt	5.09	7.9[c]	
ZnO (wurtzite)	0.81	3.43[c]	
Rock-salt	2.61		5.23*

[a] Reference [52]. [b] Reference [84]. [c] Reference [85].

known problem of the LDA, which fails quantitatively in dealing with excited-state properties. For wurtzite MgO and CdO, the expected experimental values are obtained by using the same correction for both wurtzite and rock-salt structures as Anderson *et al* assumed [52]. The same method is applied to yield the 'predicted' (or expected experimental) values for rock-salt ZnO. These experimental and 'predicted' band gaps of the bulk materials will be used to correct the band gaps of the alloy configurations.

Quasiparticle corrections for the band gap have been shown to vary almost linearly with the composition in ternary nitride alloys [75]. It is reasonable to expect that the same correction relation is valid for ternary oxide alloys. We have therefore applied a linear shift in the band gap for alloy $Mg_xZn_{1-x}O$ and $Cd_xZn_{1-x}O$ in order to match the experimental values for the band gap of the parent materials. Since the credible band gaps of wurtzite and rock-salt CaO are
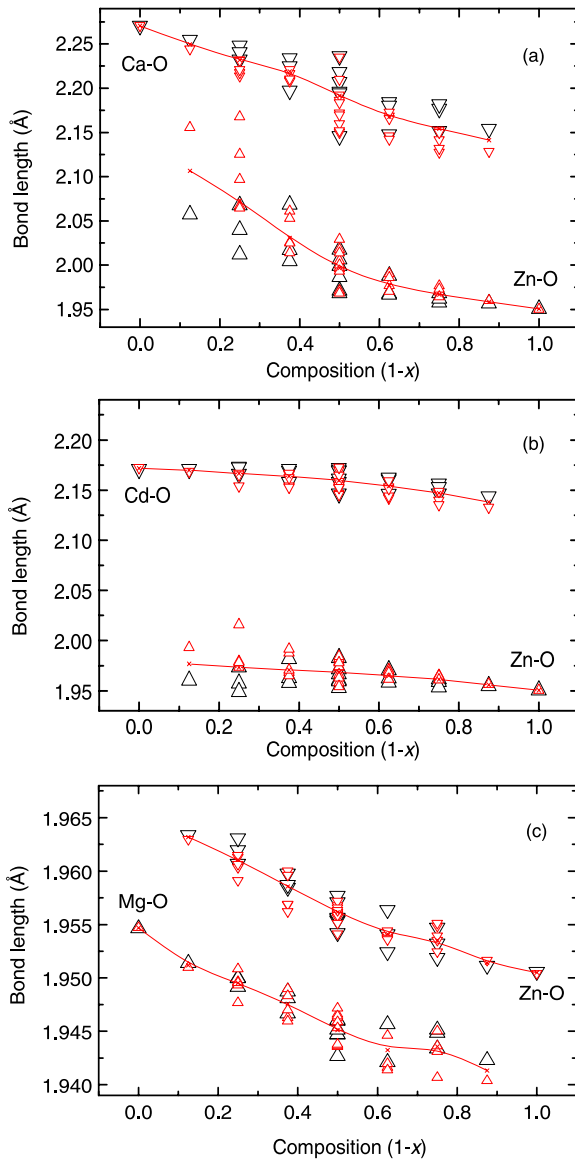
Figure 4. Nearest-neighbor bond length ($\triangle$ for A–O and $\triangledown$ for Zn–O) of the alloy configurations and averaged bond length (red line) as a function of concentration x for three alloy systems $A_xZn_{1-x}O$ (A = Ca, Cd and Mg).

not known, we have only shown the raw LDA-calculated value for $Ca_xZn_{1-x}O$.

The original calculated values, the corrected calculated values and the experimental values are illustrated in figure 5. A small downward bowing of the band gaps for the calculated values and the experimental value is clearly seen, and we will elaborate on the bowing parameter later. The band gaps of different alloy configurations with the same concentration can be quite different, for example the band gaps of $Mg_{0.5}Zn_{0.5}O$ can differ by 1 eV. This observation verifies the importance of taking the alloy statistics into account when analyzing the electronic properties. From figure 5(c), the corrected calculated band gaps of $Mg_xZn_{1-x}O$ are generally larger than the experimental values. This trend is expected and can be attributed to the fact that experimental values were obtained at room temperature and the disordered excited states existed in

the sample, that is due to the thermal effect of the process of growth. From figure 5(b), it can be seen that the experimental band gaps of $Cd_xZn_{1-x}O$ can be greater than our calculated values. This may be due to the underestimate of the theoretical band gap of the pure crystal CdO, and/or the potential errors in experimental measurements.

Because of the importance of the fundamental band gap for device design, its nonlinear dependence on the concentration calls for further qualitative understanding and quantitative analysis. Through simple theory analysis such as the perturbation scattering theory, it is considered that a quadratic function of the concentration can be used to describe the downward shift of the band gap of the alloy from the linear average, by defining a bowing coefficient b as [76]

$$E_g(A_xB_{1-x}C) = xE_{AC}(a_{AC}) + (1-x)E_{BC}(a_{BC}) - bx(1-x). \quad (5)$$

In order to deduce the bowing parameters b_{MgZnO} and b_{CdZnO}, we first calculated the averaged band gaps as a function of the concentration based on equations (4). It is apparent that the averaged band gap of 'wurtzite' $Ca_xZn_{1-x}O$ does not follow a simple quadratic form. This strange trend is linked to the instability of bulk wurtzite CaO, and we found that in the Ca-rich region the dominating structures are closer to h-CaO rather than the wurtzite phase.
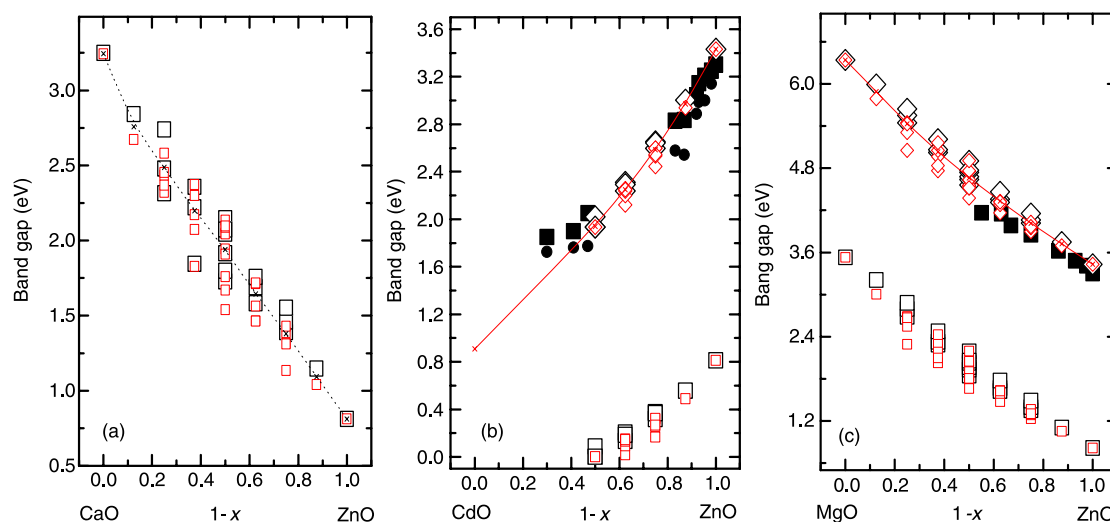
The averaged band gaps of $Mg_xZn_{1-x}O$ and $Cd_xZn_{1-x}O$ can be well fitted with formula (5), and we found that the bowing parameters are 0.87 ± 0.03 and 1.03 ± 0.05 eV for alloys $Mg_xZn_{1-x}O$ and $Cd_xZn_{1-x}O$, respectively.

4. Conclusions

In summary, we have presented systematical studies of phase stability, structural and electronic properties of three zinc-based oxide alloy systems ($Ca_xZn_{1-x}O$, $Cd_xZn_{1-x}O$ and $Mg_xZn_{1-x}O$) by first-principles total energy calculations. In order to consider the importance of the alloy statistics, the phase stability of the isovalent alloy with nonisostructural compounds is analyzed by examining all alloy configurations in three different eight-cation supercells ($1 \times 1 \times 2$ B1 phase structure, $2 \times 2 \times 1$ and $2 \times 1 \times 2$ B4 phase structures). We have used the symmetry of the bulk materials to reduce the 2^8 complexities to about 20–30 distinct alloy configurations for each supercell.

The overall mixing energies of these alloys are positive—indicating that both wurtzite and rock-salt alloy phases are not stable with respect to their parent materials. This suggests that the successful fabrication of alloys $Mg_xZn_{1-x}O$ and $Cd_xZn_{1-x}O$ with broad composition ranges should be attributed to the non-equilibrium growth condition offered by today's epitaxial growth techniques, that kinetically limits the phase separation process. $Ca_xZn_{1-x}O$ is found to be problematic, partially due to the instability of the wurtzite CaO. Taking into account the alloy statistics, we have drawn the region of phase stability for $Mg_xZn_{1-x}O$ ($0.375 < x < 0.5$) and $Cd_xZn_{1-x}O$ ($0.75 < x < 0.875$). These regions are in line with the experimental work of Vashaei *et al* [19] and Ishihara *et al* [36].

Figure 5. The band gaps as a function of concentration for three alloy systems $A_xZn_{1-x}O$ (A = Ca, Cd and Mg). LDA-calculated band gaps at the Γ point are shown as empty squares. The 'corrected' band gaps (empty diamonds) and the average 'corrected' band gaps of each concentration (red line) are compared to the experimental data (different black symbols) for alloy $Mg_xZn_{1-x}O$ [57] and $Cd_xZn_{1-x}O$ [30]. Note that the band gaps of $Ca_xZn_{1-x}O$ are not 'corrected' due to the lack of a reliable experimental value of the bulk wurtzite CaO.

The structures of the three alloys in wurtzite phase were analyzed by examining their lattice constants and averaged structure parameters (u). We found that the lattice constants of $Cd_xZn_{1-x}O$ follow the Vegard's rule, while $Mg_xZn_{1-x}O$ and $Ca_xZn_{1-x}O$ have notable deviation for $x > 70\%$ and $x > 50\%$ respectively. Inspecting the structure parameters (u), we found that the significant deviation from Vegard's rule in $Ca_xZn_{1-x}O$ is associated with the instability of the wurtzite CaO.

For alloys $Cd_xZn_{1-x}O$ and $Mg_xZn_{1-x}O$, the calculated band gaps are generally consistent with the experimental values, considering the error of experimental measurement and the veracity of the LDA correction. The bowing parameters are calculated and found to be 0.87 and 1.03 eV for alloys $Mg_xZn_{1-x}O$ and $Cd_xZn_{1-x}O$, respectively.

Acknowledgments

References

[1] Thomas D G 1960 *J. Phys. Chem. Solids* **15** 86
[2] Bagnall D *et al* 1997 *Appl. Phys. Lett.* **70** 2230
[3] Yu P *et al* 1997 *Solid State Commun.* **103** 459
[4] Tang Z K *et al* 1998 *Appl. Phys. Lett.* **72** 3270
[5] Makino T *et al* 2001 *Appl. Phys. Lett.* **78** 1237
[6] Nakamura A *et al* 2007 *Appl. Phys. Lett.* **90** 093512
[7] Segnit E R and Holland A E 1965 *J. Am. Ceram. Soc.* **48** 412
[8] Ohtomo A *et al* 1999 *Appl. Phys. Lett.* **75** 980
[9] Sharma A K *et al* 1999 *Appl. Phys. Lett.* **75** 3327
[10] Park W I, Yi G-C and Jang H M 2001 *Appl. Phys. Lett.* **79** 2022
[11] Choopun S *et al* 2002 *Appl. Phys. Lett.* **80** 1529
[12] Narayan J *et al* 2002 *Solid State Commun.* **121** 9
[13] Chen J *et al* 2003 *J. Phys.: Condens. Matter* **15** L475
[14] Takagi T *et al* 2003 *Japan. J. Appl. Phys.* 2 **42** L401
[15] Fujita S *et al* 2004 *Phys. Status Solidi* b **241** 599
[16] Norton D P *et al* 2004 *Mater. Today* **7** 34
[17] Koike K *et al* 2005 *J. Cryst. Growth* **278** 288
[18] Tanaka H, Fujita S and Fujita S 2005 *Appl. Phys. Lett.* **86** 192911
[19] Vashaei Z *et al* 2005 *J. Appl. Phys.* **98** 054911
[20] Wencstern H v *et al* 2006 *Appl. Phys. Lett.* **89** 092122
[21] Chang Y-S *et al* 2007 *J. Appl. Phys.* **101** 033502
[22] Kim Y-I, Page K and Seshadri R 2007 *Appl. Phys. Lett.* **90** 101904
[23] Ryu Y R *et al* 2006 *Appl. Phys. Lett.* **88** 052103
[24] Kim Y-S, Lee E-C and Chang K J 2001 *J. Korean Phys. Soc.* **39** S92
[25] Sanati M, Hart G L W and Zunger A 2003 *Phys. Rev. B* **68** 155210
[26] Fan X F *et al* 2007 *Appl. Phys. Lett.* **91** 121121
[27] Sakurai K *et al* 2000 *Japan. J. Appl. Phys.* **39** L1146
[28] Sakurai K *et al* 2002 *J. Cryst. Growth* **514** 237
[29] Gruber T *et al* 2003 *Appl. Phys. Lett.* **83** 3290
[30] Shigemori S *et al* 2004 *Japan. J. Appl. Phys.* 2 **43** L1088
[31] Lee S Y *et al* 2004 *Appl. Phys. Lett.* **85** 218
[32] Wang X J *et al* 2006 *Appl. Phys. Lett.* **89** 151909
[33] Bertram F *et al* 2006 *Appl. Phys. Lett.* **88** 061915
[34] Zúñiga-Pérez J *et al* 2006 *J. Appl. Phys.* **99** 023514
[35] Sun C W *et al* 2006 *Appl. Phys. Lett.* **89** 181923
[36] Ishihara J *et al* 2006 *Appl. Phys. Lett.* **89** 091914
[37] Buyanova I A *et al* 2007 *Appl. Phys. Lett.* **90** 261907
[38] Pandey R, Jaffe J E and Kunz A B 1990 *Phys. Rev. B* **43** 9228
[39] Kotani T 1994 *Phys. Rev. B* **50** 14816
[40] Yamasaki A and Fujiwara T 2002 *Phys. Rev. B* **66** 245108
[41] Koffyberg F P 1970 *Phys. Rev. B* **13** 4470
[42] Boettger J C and Kunz A B 1983 *Phys. Rev. B* **27** 1359
[43] Guerrero-Moreno R J and Takeuchi N 2002 *Phys. Rev. B* **66** 205205
[44] Karki B B *et al* 2000 *Phys. Rev. B* **61** 8793
[45] Oganov A R and Dorogokupets P I 2003 *Phys. Rev. B* **67** 224110
[46] Limpijumnong S and Jungthawan S 2004 *Phys. Rev. B* **70** 054104
[47] Serrano J *et al* 2004 *Phys. Rev. B* **69** 094306
[48] Sun J *et al* 2005 *Phys. Rev. B* **71** 125132
[49] Jaffe J E, Pandey R and Kunz A B 1991 *Phys. Rev. B* **43** 14030
[50] Jaffe J E *et al* 2000 *Phys. Rev. B* **62** 1660

[51] Gopal P and Spaldin N A 2006 *J. Electron. Mater.* **35** 538
[52] Janotti A, Segev D and Walle C G V d 2006 *Phys. Rev.* B
      74 045202
[53] Schleife A *et al* 2006 *Phys. Rev.* B **73** 245212
[54] Janotti A and Walle C G V d 2007 *Phys. Rev.* B
      75 121201(R)
[55] Parthe E 1964 *Crystal Chemistry of Tetrahedral Structures*
      (New York: Gordon and Breach)
[56] Parthe E 1964 *Crystal Chemistry of Tetrahedral Structures*
      (New York: Gordon and Breach)
[57] Ohtomo A *et al* 1998 *Appl. Phys. Lett.* **72** 2466
[58] Ehrenreich H and Schwartz L M 1976 *Solid State Physics*
      ed H Ehrenreich, F Seitz and D Turnbull (New York:
      Academic)
[59] Zunger A *et al* 1990 *Phys. Rev. Lett.* **65** 353
[60] Wei S H *et al* 1990 *Phys. Rev.* B **42** 9622
[61] Chen A B and Sher A 1995 *Semiconductor Alloys: Physics and
      Material Engineering* (New York: Plenum)
[62] Hohenberg P and Kohn W 1964 *Phys. Rev.* **136** B864
[63] Kohn W and Sham L J 1965 *Phys. Rev.* **140** A1133
[64] Blöchl P E 1994 *Phys. Rev.* B **50** 17953
[65] Kresse G and Joubert D 1999 *Phys. Rev.* B **59** 1758
[66] Kresse G and Hafner J 1993 *Phys. Rev.* B **47** 558
[67] Kresse G and Furthmuller J 1996 *Phys. Rev.* B **54** 11169
[68] Kresse G and Furthmuller J 1996 *Comput. Mater. Sci.* **6** 15
[69] Monkhorst H J and Pack J D 1976 *Phys. Rev.* B **13** 5188
[70] Limpijumnong S and Lambrecht W R L 2001 *Phys. Rev.* B
      63 104103
[71] Seko A *et al* 2005 *Phys. Rev.* B **72** 024107
[72] Vegard L 1921 *Z. Phys.* **5** 17
[73] Sarver J F, Katnack F L and Hummel F A 1959 *J. Electrochem.
      Soc.* **106** 960
[74] Malashevich A and Vanderbilt D 2007 *Phys. Rev.* B **75** 045106
[75] Sökeland F *et al* 2003 *Phys. Rev.* B **68** 075203
[76] Bernard J E and Zunger A 1987 *Phys. Rev.* B **36** 3199
[77] Pichet P, Mao H K and Bell P M 1988 *J. Geophys. Res.*
      93 15279
[78] Decremps F *et al* 2003 *Phys. Rev.* B **68** 104101
[79] Zhang J 1999 *Phys. Chem. Minerals* **26** 644
[80] Karzel H *et al* 1996 *Phys. Rev.* B **53** 11425
[81] Landolt-Börnstein 1975 *Numerical Data and Functional
      Relationships, Crystal Structure Data of Inorganic
      Compounds* (Berlin: Springer)
[82] Recio J M *et al* 1998 *Phys. Rev.* B **58** 8949
[83] Desgreniers S 1998 *Phys. Rev.* B **58** 14102
[84] Koffyberg F P 1976 *Phys. Rev.* B **13** 4470
[85] Madelung O 2003 *Semiconductor: Data Handbook*
      (New York: Springer)